LUPINE PUBLISHERS

Modern Approaches on Material Science

DOI: 10.32474/MAMS.2021.03.000173

ISSN: 2641-6921

Research Article

A Novel Approach for the Decoration of Parylene C Coatings Using Functional Silica-Triclosan Co-Polymer Nanoparticles

Rina B Binyamini[1], Edith Laux[2], Herbert Keppner[2] and Jean Paul Lellouche[1]*

[1]*Department of Chemistry, Faculty of Exact Sciences, Institute of Nanotechnology and Advanced Materials (BINA), Bar-Ilan University, Israel*

[2]*Haute Ecole Arc Ingénierie (HES-SO), CH-2300 La Chaux-de-Fonds, Switzerland*

***Corresponding author:** Jean-Paul Lellouche, Department of Chemistry, Faculty of Exact Sciences, Bar-Ilan University, Ramat Gan 5290002 Israel Institute of Nanotechnology and Advanced Materials (BINA), Bar-Ilan University, Ramat Gan, 5290002, Israel

Received: February 23, 2021 **Published:** March 03, 2021

Abstract

Both pure silica (SiO_2) nanoparticles (SNPs) and functionalized hybrid triclosan (TCS)/silica nanocomposites (T-SNCs) were deposited onto nonfunctional Parylene C films using a novel, readily executed, one-step decoration method. Unlike previously known methods, this functionalization method of Parylene C films required neither any binding agent nor sophisticated equipment/devices. The SiO_2-based NPs anchored onto Parylene C substrates were formed via a common base-catalyzed hydrolytic sol-gel method. Regarding the mechanism, it has been assumed that the SiO_2 phase precursor ($Si(OC_2H_5)_4$), tetraethoxysilane (TEOS), was first adsorbed and 2D polymerized onto the parylene C film due to hydrophobic interactions that served as an anchor mechanism for further corresponding NPs growth [1] This assumption was investigated by comparing thermal behaviors (measured by differential scanning calorimetry, DSC) of parylene C coatings before and after the following specific surface treatment, i.e., first (i) first parylene C coating incubation with TEOS, followed by (ii) SNPs formation and growth from such a TEOS-modified coating surface. Following the same procedure, hybrid thiophene-containing H-SiO_2-TCS NPs were also successfully grown from the surface of a same TEOS-modified parylene C film and characterized using high resolution scanning electron microscopy (HR-SEM) and X-ray photoelectron spectroscopy (XPS). In order to obtain deeper insight into the overall functionalization process, the similar hybrid H-SiO_2-TCS NPs that formed in the bulk-contacting medium were also isolated and fully characterized for comparison needs. Resulting anti-bacterial biological experiments were also performed as well.

Keyword: Silica nanoparticles; hybrid silica/thiophene nanoparticles; functional parylene c coatings; hybrid silica-perylene c composites; antibacterial parylene c coatings

Introduction

The current deliverable issues with the subject of Parylene composite films modified with antibacterial coatings. In this study, we report on the design, synthesis, and characterization of covalently linked, triclosan silica-based nanocomposites (TCS-SNCs). In the context of increased bacterial resistance to common antibiotic treatments, nanoscale materials offer a unique opportunity to bring innovative and more effective solutions to bacterial disease control. Currently, several options have already been successfully explored using various types of organic/inorganic and composite nanomaterials. For example, such options include:

a) Silver (Ag) nanoparticles (NPs) [2].

b) Carbon-based nanomaterials like single- walled carbon nanotubes (SWCNTs),[3] C60 fullerenes, and graphene oxide;[4].

c) FDA-approved bioactive glasses (SiO_2–Na_2O–CaO–P_2O_5) of the 45S5 type, [2].

d) Metal oxide (TiO_2, MgO, ZnO) NPs, [2,4] magnesium fluoride (MgF_2) NPs, [5] and

e) Chemically modified (antibiotic-decorated) gold (Au) NPs [6,7].

Each of these optional nanoscale systems clearly possesses its own specific mechanism of action, cellular target(s), potential delivery capability, and overall therapeutic advantages and disadvantages. Triclosan (TCS) is a well-known commercial and Food and Drug Administration (FDA)-approved, synthetic, nonionic, broad-spectrum antimicrobial agent [6]. It mainly possesses antibacterial, but also some parallel antifungal and antiviral properties [7-9]. Numerous studies conducted on different bacteria

strains showed that TCS acts on a defined bacterial target in the bacterial fatty acid biosynthetic pathway, the NADH-dependent enoyl- [acyl carrier protein] reductase (ENR) [10-15].

Loading triclosan into an organic or inorganic matrix to induce antibacterial properties has been extensively researched [16,17]. For this goal, different polymers and nanomaterials have been used, such as polystyrene, [18-20] TiO_2 particles to learn about the sustained release of antibacterial materials, [21-25] β-cyclodextrin bacteria-growth resistance [26,27] and loaded into poly(D,L-lactide-co- glycolide) (PLGA) [28-30], poly(D, L-lactide) (PLA) [31-35] and poly(vinyl alcohol) (PVAL) copolymers for periodontal disease, etc. [36,37] Triclosan-loaded NPs (TiO_2 nanocapsules) have also been prepared, but triclosan has never been covalently bound to an inorganic matrix. In this novel study, we developed a specific linker that will allow covalent binding between silica NPs and triclosan. The covalent bond between the linker and the biocide has been designed to be broken/hydrolyzed by enzymes, subsequently releasing the active triclosan, which will act upon its target inside the cell. Basically, the enzymes produced by the bacteria themselves will be responsible for the release of this antimicrobial agent. Such a covalent linkage ensures the above-mentioned properties and also prevents leaching, providing an improved mechanism for controlled release. In this context, parylene-type polymers are characterized by their high solvent resistance, low dielectric constant, good barrier properties, full biocompatibility, and ability to be readily deposited by chemical vapor deposition (CVD) via thermal cracking of (2,2)-paracyclophane monomers [38,39]. Furthermore, parylene C (poly(monochloro-para-xylylene)) has a high permeability resistance to common gases, i.e., H_2O, N_2, and O_2, while exhibiting a high elastic modulus [40]. These exceptional combined properties promote parylene C as an ideal coating polymer for microelectronic devices, medical instruments, implants, and numerous other applications [1, 41-46]. Herein, we report about the design and synthesis of parylene C composite films modified with antibacterial coatings, using the innovative linker triclosan-(3-(triethoxysilyl) propyl) carbamate (TTESPC), and the resulting nanosized, silica-based particles onto parylene films. Each particle contains the FDA-approved antibacterial agent triclosan, covalently linked within the matrix for its controlled slow release upon interaction. The particles were prepared according to a modified Stöber method, and the biocide-silanated linker was incorporated into the silica matrix during the particle-formation process.

Experimental Section

Triclosan-(3-(triethoxysilyl)propyl) carbamate (TSC-linker) synthesis

Triclosan (5-chloro-2- (2,4-dichlorophenoxy) phenol) (1 g, 3.45 mmol, 1 eq.) and dry toluene (5.0 mL) were added to a three-necked round-bottom flask under an N_2 atmosphere, to obtain a 0.7 M solution. 3-(Triethoxysilyl) propyl isocyanate (1.28 mL, 5.18 mmol, 1.5 eq.) and tetraoctyltin (3.02 ml, 5.18 mmol, 1.5 eq.) were added simultaneously to the reaction mixture, which was stirred at room temperature until no progress in the reaction could be observed by thin layer chromatography (TLC) (4:1 n-hexane: EtOAc) n-hexane: ethyl acetate (EtOAc)). Toluene was evaporated until off-white oil emerged. Upon crystallization overnight, white crystals were obtained. These were filtered with cold n-hexane to remove traces of the stannane complex and dried under vacuum to yield 63.5% (1.17 g) of a white crystalline powder. The TTESPC melting point is about 83-84°C. (Scheme 1)

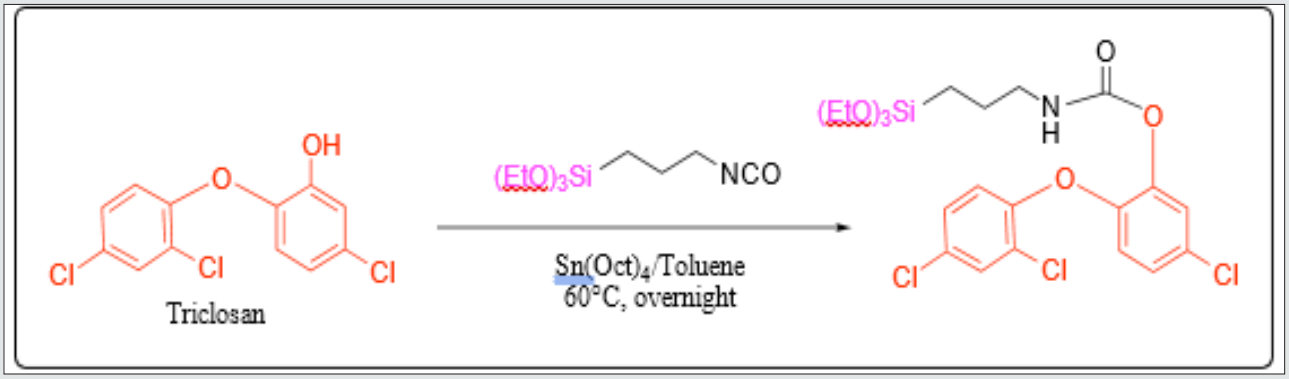

Scheme 1: Synthetic pathway for the fabrication of the TTESPC linker according to this noticed specific former article/synthetic methodology.

Parylene C films modified with Triclosan-silica nanocomposites (TCS-SNCs)

There are several ways to incorporate molecules into a sol-gel system [47-49]. The first is the physical incorporation of drug substances, drug loading for example, into sol-gel-derived silica materials. This method was first introduced in 1983 [50]. We designed and fabricated onto the parylene C surface novel hybrid-silica nanoparticles containing the FDA-approved antimicrobial triclosan (Irgasan) covalently linked within the inorganic matrix for its controlled slow release upon interaction. The full characterization of the triclosan-silica nanocomposites (T-SNCs) onto the Parylene C film, triclosan-(3- (triethoxysilyl)propyl) carbamate (TCS linker),

and their appropriate linkers is accomplished by thermogravimetric, microscopic, and spectroscopic techniques.

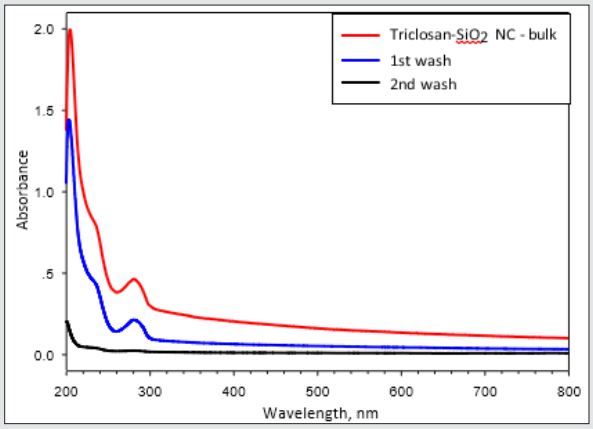

Figure 1: UV spectroscopy analysis of washing media arising from the synthesis of triclosan-loaded silica nanocomposites onto the Parylene C film..

Parylene films modified with a different ratio of Triclosan-silica nanocomposites (TCS-NCs): Parylene film (1.5×1.5cm), previously cleaned in an ultrasonic bath for 15 minutes with acetone, was placed in a reaction vessel containing 10 ml of ethanol. Then, 0.53 ml of ammonium hydroxide and 1.5 ml (6.72 mmol) of tetraethyl orthosilicate (TEOS) were added (Scheme 1). The reaction was mixed for 3 minutes and then different amounts of the TTESPC linker: 36 mg (1%), 108 mg (3%), and 180 mg (5%), which were previously dissolved in 2 mL ethanol, were added to the reaction vials. The reaction was performed at room temperature for 24 h with constant agitation using an orbital shaker. The resulting generated silica-modified film was washed with ethanol and then washed again in ethanol for 10 min using an ultrasonic bath (Elmasonic S 30 ultrasonic bath, 37 kHz at full power irradiation), three times, in order to remove physically adsorbed silica particles. The film was then air-dried. The decorated Parylene C was washed three times in an ultrasonic bath, each time for 10 minutes, using analytical grade EtOH. Thus, all the obtained composite washing solutions were UV tested (measurement scale: 200-800 nm, detection of conjugated triclosan chromophore/species) to detect the presence of triclosan-loaded silica nanocomposites. As clearly deduced from the (Figure 1) data, the second wash step already disclosed no UV-based evidence at all for the presence of any further free UV-absorbing triclosan molecules and/or triclosan silica nanocomposites. (Figure 2) shows micrographs of high-resolution scanning-electron microscopy (HRSEM) of the TCS-SNCs obtained in a typical experiment at room temperature with 2.5% (w/v) of TTESPC. One can appreciate from these micrographs the smooth, spherical morphology of the NPs. These nanocomposites were obtained with a narrow size distribution and an average diameter of 130 ± 30 nm (at dry measurements). DLS studies showed a hydrodynamic diameter of 164.3 nm (Figure 3), which is in a good accordance with the actual TEM size of similar dried particles, when considering the likely adsorption of water molecules onto the NC surface.

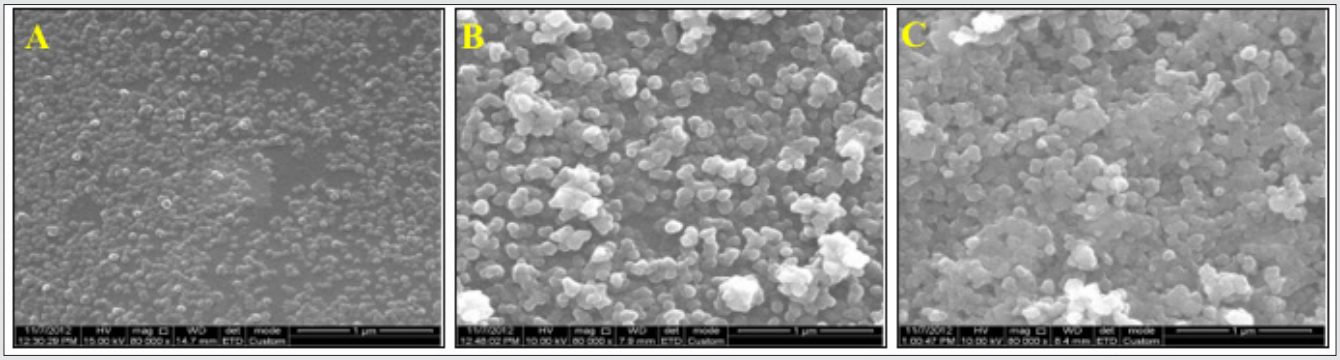

Figure 2: HRSEM images of Parylene C films with different concentrations of TCS-linker in the presence of 1.5 ml, TEOS (10 ml EtOH, 0.53 ml NH4OH) at room temperature: 1% (A), 3% (B), and 5% (C). Magnification x80K.

A comparison of the Parylene C film coverage by the triclosan-silica nanocomposites (T-SNC) using different TTESPC concentrations at room temperature revealed a proper coverage of the film by the nanocomposites. Nonetheless, the nanocomposites at the lower concentration (1%, Figure 2A) seem to be concentrated in clusters, hence there are bare areas of Parylene C film, while with other TTESPC concentrations (3% and 5%, Figures 1-B & 1-C respectively), the TCS- NC creates a complete coverage of the film. Triclosan-silica nanocomposites (TCS-NCs) were synthesized onto Parylene C film at room temperature. The content of the triclosan linker varied from 1%, 3%, and 5%. The diameter of the nanocomposites was measured using ImageJ software on HRSEM images. The size distribution of such nanocomposites assembled with a 1% triclosan linker was from 100 to 149nm, while when using a 3% triclosan linker, it yielded nanocomposites with the size range of 70 to 129 nm, while nanocomposites of the 5% one varied from 140 to 199nm.

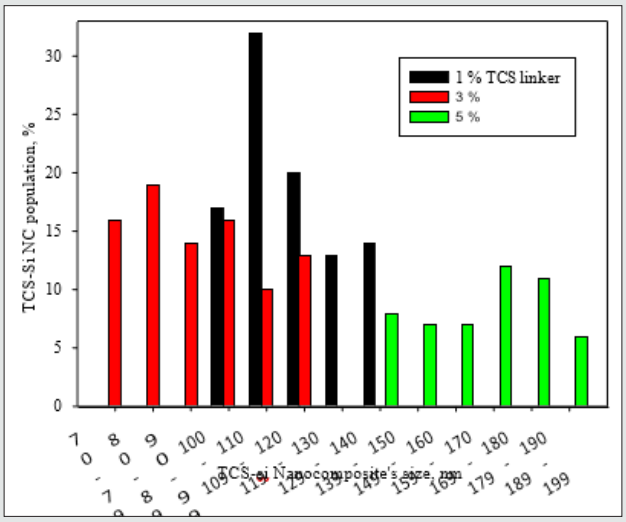

Figure 3: Size measurements of different concentrations (1%, 3%, and 5%) of triclosan linker into the triclosan-silica nanocomposites (TCS-NCs) at room temperature. Size measurements were carried out using ImageJ software for HRSEM images. From each concentration, 200 nanocomposites were sampled for size measurements.

3-Parylene films modified with different ratio of Triclosan-silica nanocomposites (TCS- NCs) at 60 ˚C: We were inspired to reduce the diameter and size distribution of the triclosan-silica NPs that were synthesized on the parylene film. Parylene film (10 μm thickness, third part of the microscope slide) previously cleaned in an ultrasonic bath for 15 minutes with acetone was placed in a reaction vessel containing 10 ml of ethanol. Then, 0.53 ml of ammonium hydroxide and 1.5 ml (6.72 mmol) of TEOS were added. The reaction was mixed for 3 minutes and then different amounts of TTESPC: 1%, 3%, and 5% (previously dissolved in ethanol), were added to the reaction vessel. The reaction was performed at 60˚C for 24h with constant agitation by an orbital shaker. The resulting silica modified film was washed with ethanol and then washed again in ethanol for 10 min using an ultrasonic bath (Elmasonic S 30 ultrasonic bath, 37 kHz at full power irradiation) three times, to remove physically adsorbed silica particles. The film was then air-dried. (Figures 4 & 5) An additional FTIR analysis (Figure 6) supports this data, since it discloses the similar chemical composition of the triclosan-silica nanocomposites synthesized onto Parylene C film (Figure 6) top). The IR spectrum of Parylene C film at 2830-3027 cm^{-1} which correspond to C-H stretching bands are screened by the TCS-NCs, therefore almost invisible after the synthesis of the nanocomposites. The IR spectrum of the triclosan-silica nanocomposites (Figure 6 top) reveals peaks, which are characteristic of the SiO_2 phase (1110 cm^{-1}, 3000-3800 cm^{-1}, etc.) as well as a distinguished peak for C-Cl at 550 - 800 cm^{-1} (see scheme 1). H-SiO_2-Th NPs produced in the bulk solution in presence of parylene film (Figure 7C) shows the same set of peaks as the spectrum of the H-SiO_2-Th NPs prepared in absence of parylene as opposed to the spectrum of SiO_2 NPs (Figure 7A), which exhibits only the peaks characteristic to SiO_2 NPs (1110 cm^{-1}, 3000-3800 cm^{-1}, etc.).

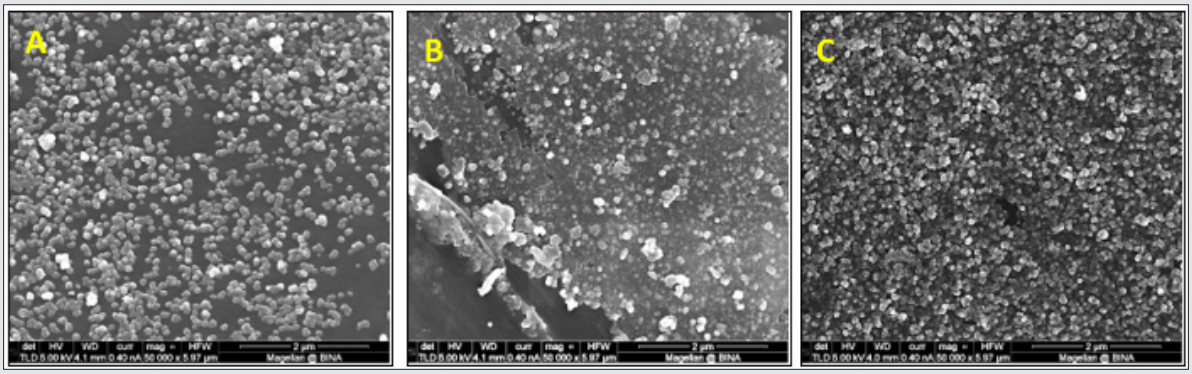

Figure 4: HRSEM images of Parylene C films with different concentrations of TCS-linker in the presence of 1.5 ml TEOS (10 ml EtOH, 0.53 ml NH4OH) at 60 °C: 1% (A), 3% (B), and 5% (C). Magnification x50K.

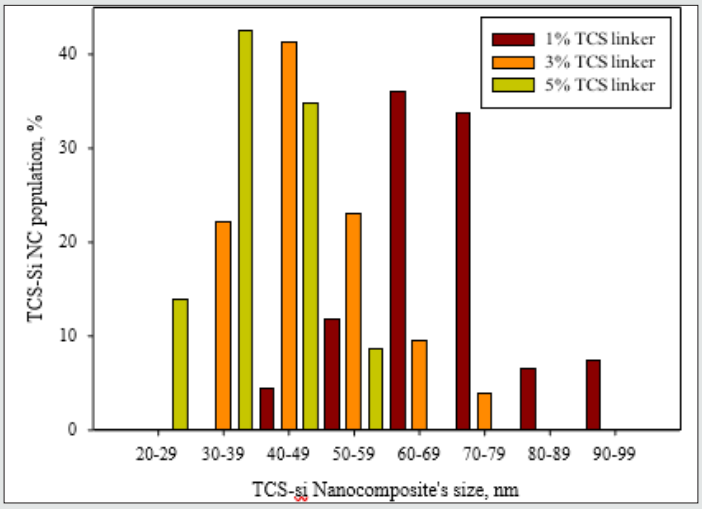

Figure 5: Size measurements of different concentrations (1%, 3%, and 5%) of the triclosan linker into the triclosan-silica nanocomposites (TCS-NCs) at 60 °C. Size measurements were carried out using ImageJ software for HRSEM images. From each concentration, 200 nanocomposites were sampled for size measurements.

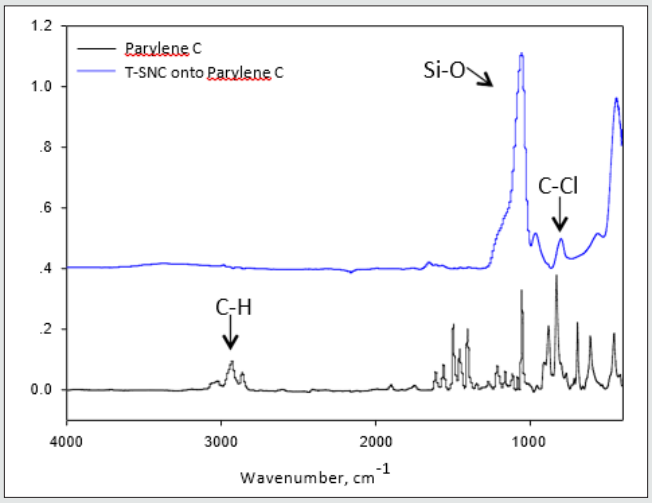

Figure 6: FTIR spectra of Parylene C film (bottom) and TCS-NCs synthesized onto Parylene C film (top).

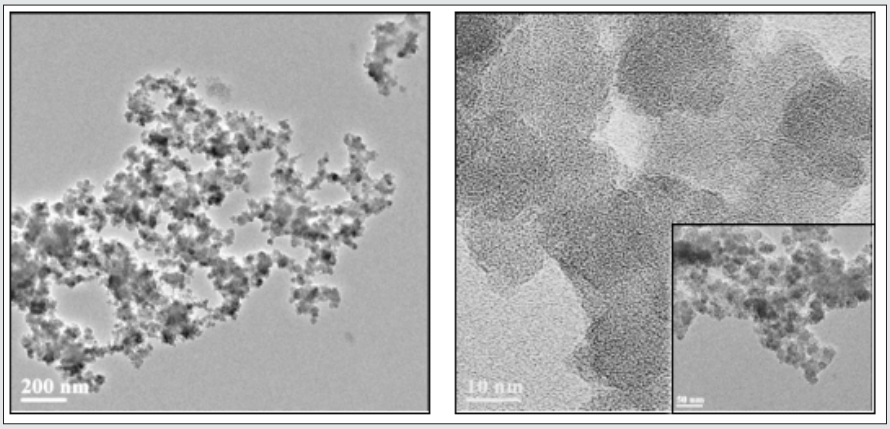

Figure 7: HRTEM images of triclosan-silica nanocomposites, which were synthesized.

Nanoparticles from the bulk: During the synthesis of triclosan-silica nanocomposites (TCS-NCs) onto Parylene C film (see section 3.2), triclosan-silica nanocomposites were being synthesized in the medium as well as onto the Parylene C film. The TCS-NCs were collected from the medium and characterized by varied methods such as: Zeta potential, elemental analysis, thermogravimetric analysis, Differential scanning calorimetry and High Resolution TEM (Figures 7 & 8). The FTIR image shows the Fourier transform IR spectra of triclosan linker-silica nanocomposites (TCS-SiO_2/NCs), which were isolated from the reaction solution. We can clearly identify characteristic peaks of the functional groups of the silica and the triclosan. The IR spectrum of the triclosan linker-silica nanocomposites (TCS-SiO_2/NCs) shows a broad curve with a peak at 3390 cm^{-1}, which corresponds to the carbamate NH and alkane CH_2 asymmetric- stretching bands, a small peak at 1639 cm^{-1} which stands for the carbamate C=O stretching band, a broad curve with a peak at 1108 cm^{-1} (Si-O-C ether stretching bands, aromatic C=C stretching bands and phenolic symmetrical C-O stretching bands), a peak at 949 cm^{-1} (aromatic C-H stretching bands), and a peak at 789 cm^{-1} (C-Cl stretching bands) [51]. The elemental analysis summarized in (Figure 9), since these measurements relate to the Parylene C film, The T-SNC attached and not attached onto the film and to the triclosan linker itself. The Parylene C film consists of carbon rings,[1] so it is quite obvious that the highest elevation of the carbon element was found at the T-SNCs onto the Parylene C film samples and the lowest carbon content was found at the T-SNPs. This complete set of results clearly demonstrates the main advantages of this mild functionalization method for obtaining stable and efficiently grown grafted SiO_2 NPs onto the parylene C substrate. This is a simple and mild one-step procedure that requires neither special equipment nor binding agent. It is entirely likely that such a method might be performed using various other kinds of silica-based precursors. These results clearly emphasize the advantages of this specific functionalization method, i.e., a simple one-step delivery of a stable and effective deposition/growth of bare silica NPs onto a parylene C substrate. Moreover, this wet chemistry procedure is operated without using any special equipment or binding chemical agents and might possibly be extended to other kinds of different silicate precursors as illustrated below.

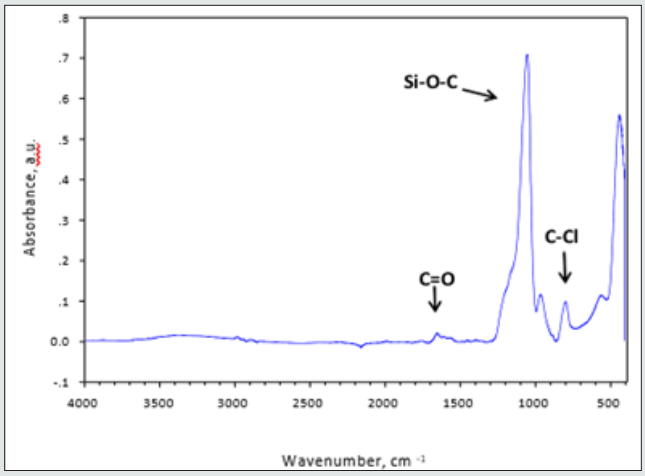

Figure 8: FTIR image of co-polymer from the solution.

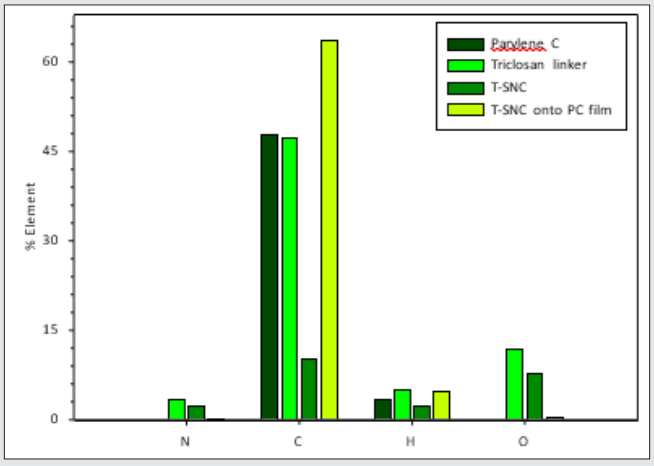

Figure 9: Elemental Analysis of Parylene C film, TCS linker, TCS-NCs from the medium and TCS-NCs

Biological Results

The antimicrobial activity of NPs-coated Parylene C films was evaluated using both Escherichia coli ATCC 25922 and triclosan-resistant strain RJH 108. Both bacteria were grown overnight in Nutrient Broth (NB, Sigma) media under shaking (250 rpm) at 37 ˚C. On the following day, the overnight cultures were each diluted in a fresh NB medium to obtain stock solutions with a working concentration of 105 colony-forming units (CFU) per ml. Each of the parylene-modified coatings (1 cm diameter) was exposed to 1 ml of either of the bacterial stock solutions in a 24- well plate (DE-GROOTH). The plates were then incubated at 37 °C for 24 h. On the following day, in order to determine the CFU parameter in each treatment, serial dilutions were carried out and the cells were spotted onto NB agar plates. The NB plates were incubated at 37 °C for 20 hours. The cell growth was monitored and determined by viable cell count. The antibacterial properties of triclosan-silica nanocomposites (TCS-NCs) coated surfaces were tested against E. coli, a common bacterial pathogen, which was either sensitive to triclosan or resistant to it. As shown in (Figure 10), TCS-NCs-coated Parylene samples managed to kill all the tested bacteria within 2-4 hours as opposed to uncoated Parylene C coupons or to TCS-NCs coated Parylene samples that were incubated with triclosan-resistant E. coli (Figure 11), and as expected, did not kill the bacteria even within 24 hours.

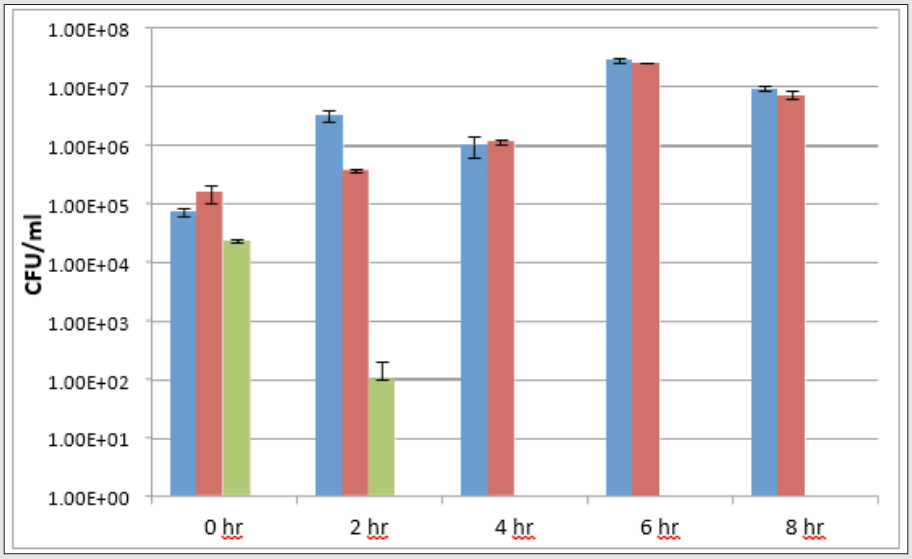

Figure 10: FTIR image of co-polymer from the solution.

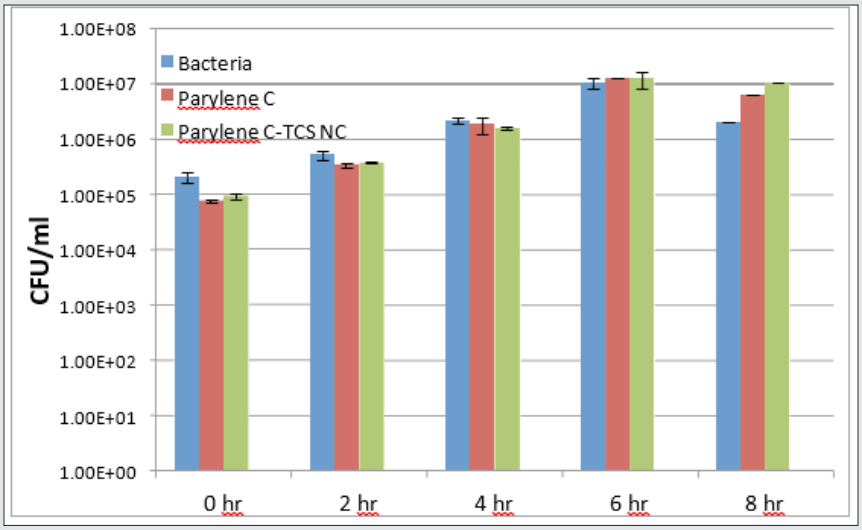

Figure 11: Triclosan-resistant strain (**B**-*below*) were grown and treated with the various surfaces as described in the methods section.

Conclusion

Triclosan-silica nanocomposites (TCS-NCs) were deposited on the surface of Parylene C by a one-step simple effective decoration method. The size of the observed generated functional NPs and their distribution on the substrate are both affected by the solution temperature, the concentration of tetraethyl orthosilicate (TEOS) [1], and the triclosan linker part in the solution. The best deposition is obtained as respect to the elevation in the temperature (from room temperature to 60 ˚C) and at 3% amount level triclosan linker. The particle-size distribution study showed that, at 3% linker level and 60oC, the generated particles were in a 30-80 nm size range. The HRSEM images also show that when using these specific conditions for coating modification, the generated TCS-NCs are effectively and homogenously dispersed onto the surface of support Parylene C films. The IR analyses of both coated and uncoated Parylene C films confirm the presence of the triclosan species onto the hybrid-modified surface. These results highlight the potential use of Triclosan-silica nanocomposites-coated surfaces for various biomedical applications.

Acknowledgement

This research has been fully supported by the European Commission through the FP 7th collaborative RTD European Project PARYLENS (FP7-NMP-2009-SMALL-3 area, contract no 246362).

References

1. Binyamini RBS, Boguslavsky Y, Laux E, Keppner H, Lellouche JPM (2015) A simple one-step approach to the decoration of parylene C coatings using functional silica-based NPs. Surf Coat Technol 263: 36-43.
2. Matthews L, Kanwar RK, Zhou S, Punj V, Kanwar JR (2010) Synthesis, characterization, and antimicrobial activity of an ampicillin-conjugated magnetic nanoantibiotic for medical applications. The Open Tropical Medicine Journal 3: 1-9.
3. Bakhsheshi Rad HR, Chen X, Ismail AF, Aziz M, Abdolahi E, et al. Improved antibacterial properties of an Mg-Zn-Ca alloy coated with chitosan nanofibers incorporating silver sulfadiazine multiwall carbon nanotubes for bone implants (2019) Polym Adv Technol 30: 1333-1339.
4. Niu A, Han Y,Wu J, Yu N, Xu Q (2010) Synthesis of one-dimensional carbon nanomaterials wrapped by silver nanoparticles and their antibacterial behavior. The Journal of Physical Chemistry C, 114: 12728-12735.
5. Akhavan O, Ghaderi E (2010) Toxicity of Graphene and Graphene Oxide Nanowalls Against Bacteria ACS Nano 4: 5731-5736.
6. Hu W, Peng C,Luo W,Lv M, Li X, et al. (2010) Graphene-based antibacterial paper. ACS Nano 4: 4317-4323.
7. Hajkova P, Spatenka P, Horsky J, Horska I, Kolouch A (2007) Photocatalytic Effect of TiO_2 Films on Viruses and Bacteria. Plasma Processes and Polymers 4: S397-S401.
8. Lellouche J, Kahana E, Elias S, Gedanken A, Banin E (2009) Antibiofilm activity of nanosized magnesium fluoride. Biomaterials 30: 5969- 5978.
9. Kumar SA, Chang YT, Wang SF, Lu HC (2010) Multifunctional Gold Nanoparticles: A Novel Nanomaterial for Various Medical Applications and Biological Activities. J Phys Chem Solids 71: 1484-1490.
10. Mao R, Huang C, Zhao X, Ma M, Qu J (2019) Dechlorination of triclosan by enhanced atomic hydrogen-mediated electrochemical reduction: Kinetics, mechanism, and toxicity assessment. Applied Catalysis B: Environmental 241: 120-129.
11. Jones RD, Jampani HB, Newman JL, Lee AS (2000) Triclosan: a review of effectiveness and safety in health care settings. American Journal of Infection Control 28: 184-196.
12. Brambilla E, Ionescu A, Cazzaniga G, Edefonti V, Gagliani M (2014) The influence of antibacterial toothpastes on in vitro Streptococcus mutans biofilm formation: a continuous culture study. Am J Dent 27: 160-166.
13. Cichocki F, Hamilton M, Ming X (2014) Google Patents.
14. McMurry LM, Oethinger M, Levy SB (1998) Triclosan targets lipid synthesis. Nature 394: 531-532.
15. Levy CW, Roujeinikova A, Sedelnikova S, Baker PJ, Stuitje AR, et al. (1999) Molecular basis of triclosan activity [9] Citation formats. Nature 398: 383-384.
16. Heath RJ, Rubin JR, Holland DR, Zhang E, Snow ME, et al. (1999) Mechanism of triclosan inhibition of bacterial fatty acid synthesis. J Biol Chem 274: 11110-11114.
17. Baldock C, Rafferty JB, Stuitje AR, Slabas AR, Rice DW (1998) The X-ray structure of Escherichia coli enoyl reductase with bound NAD^+ at 2.1 A resolution. J Mol Biol 284: 1529-1546.
18. Montazer M, Alimohammadi F, Shamei A, Rahimi MK (2012) Durable antibacterial and cross-linking cotton with colloidal silver nanoparticles and butane tetracarboxylic acid without yellowing. Colloids and Surfaces B: Bio interfaces 89: 196-202.
19. Howse GL, Bovill RA, Stephens PJ, Osborn HMI (2019) Synthesis and antibacterial profiles of targeted triclosan derivative. European Journal of Medicinal Chemistry 162: 51-58.
20. Su Y, Zhao L, Meng F, Qiao Z, Yao Y, et al. (2018) Surface-Adaptive, Antimicrobially Loaded, Micellar Nanocarriers with Enhanced Penetration and Killing Efficiency in Staphylococcal Biofilms. Materials Science and Engineering: C 93: 921-930.
21. Ramesh S, Sivasamy A, Rhee KY, Park SJ, Hui D (2015) Preparation and characterization of maleimide-polystyrene/SiO_2-Al_2O_3 hybrid nanocomposites by an in-situ sol-gel process and its antimicrobial activity. Composites Part B: Engineering 75: 167-175.
22. Cong Y, Xia T, Zou M, Li Z, Peng B, et al. (2014) Mussel-inspired polydopamine coating as a versatile platform for synthesizing polystyrene/Ag nanocomposite particles with enhanced antibacterial activities. Journal of Materials Chemistry B 2: 3450-3461.
23. Guo L, Ren S, Qiu T, Wang L, Zhang J, et al. (2015) J Nanopart Res 17: 1-14.
24. Chang YY, Lai CH, Hsu JT, Tang CH, Liao WC, et al. Analyses of Antibacterial Activity and Cell Compatibility of Titanium Coated with a Zr-C-N Film. (2012) Clin Oral Invest 16: 95-100.
25. Peyre J, Humblot V, Méthivier C, Berjeaud JM, Pradier CM (2012) Co-grafting of amino-poly(ethylene glycol) and Magainin I on a TiO_2 surface: tests of antifouling and antibacterial activities. The Journal of Physical Chemistry B 116: 13839-13847.
26. Ng A, Chan C, Guo M, Leung Y, Djurišić A, et al. (2013) Toxicity of ZnO and TiO_2 to Escherichia coli cells. Appl Microbiol Biotechnol 97: 5565-5573.
27. Montazer M, Seifollahzadeh S (2011) Enhanced Self-cleaning, Antibacterial and UV Protection Properties of Nano TiO_2 Treated Textile through Enzymatic Pretreatment. Photochem. Photobiol 87: 877-883.
28. Selvam S, Rajiv Gandhi R, Suresh J, Gowri S, Ravikumar S, et al. (2012) Antibacterial effect of novel synthesized sulfated β-cyclodextrin crosslinked cotton fabric and its improved antibacterial activities with ZnO, TiO_2 and Ag nanoparticles coating. Int J Pharm 434: 366-374.

29. Sun X, Sui S, Ference C, Zhang Y, Sun S, et al. (2014) J Agric Food Chem 62: 8914-8918.

30. Hild N, Tawakoli PN, Halter JG, Sauer B, Buchalla W, et al. (2013) Moh Acta Biomaterialia 9: 9118-9125.

31. Hill LE, Taylor TM, Gomes C (2013) Antimicrobial efficacy of poly (DL-lactide-co-glycolide) (PLGA) nanoparticles with entrapped cinnamon bark extract against Listeria monocytogenes and Salmonella typhimurium. J Food Sci 78: N626-N632.

32. Correia R, Jozala A, Martins K, Penna T, Duek E, et al. (2015) Poly (glycolic acid) (PGA): a versatile building block expanding high performance and sustainable bioplastic applications. World J Microbiol Biotechnol p. 1-11.

33. Kayaci F, O OC, Umu O, Tekinay T, Uyar T (2013) Antibacterial Electrospun Poly (lactic acid) (PLA) Nanofibrous Webs Incorporating Triclosan/ Cyclodextrin Inclusion Complexes. J Agric Food Chem 61: 3901-3908.

34. Sardo C, Nottelet B, Triolo D, Giammona G, Garric X, et al. (2014) Synthesis of three-dimensional porous hyper-crosslinked polymers via thiol-yne reaction. Coudane, Biomacromolecules 15: 4351-4362.

35. Munteanu B, Aytac Z, Pricope G, Uyar T, Vasile C (2014) J Nanopart Res 16: 1-12.

36. Kurtycz P, Karwowska E, Ciach T, Olszyna A, Kunicki A (2013) Biodegradable polylactide (PLA) fiber mats containing Al2O3-Ag nanopowder prepared by electrospinning technique-Antibacterial properties. Fibers Polym 14: 1248-1253.

37. Li X, Kanjwal MA, Lin L, Chronakis IS (2015) Electrospun polyvinyl-alcohol nanofibers as oral fast-dissolving delivery system of caffeine and riboflavin. Colloids and Surfaces B: Biointerfaces 103: 182-188.

38. Padil VVT, Černík M (2016) Green Synthesis: Nanoparticles and Nanofibres Based on Tree Gums for Environmental Applications. J Hazard Mater 287: 102-110.

39. Wen L, Wouters K, Ceyssens F, Witvrouw A, Puers R (2012) Sensors and Actuators A: Physical 186: 289-297.

40. Gorham WF (1966) Journal of Polymer Science Part A-1: Polymer Chemistry 4: 3027-3039.

41. Chiang CC, Wuu DS, Lin HB, Chen YP, Chen TN, et al. (2006) Deposition and permeation properties of SiNX/parylene multilayers on polymeric substrates. Surf Coat Technol 200: 5843-5848.

42. Pruden KG, Sinclair K, Beaudoin S (2003) Characterization of parylene-N and parylene-C photooxidation. J Polym Sci Part A: Polym Chem 41: 1486-1496.

43. Vaeth KM, Jensen KF (2000) Poly (p-phenylene vinylene) Prepared by Chemical Vapor Deposition: Influence of Monomer Selection and Reaction Conditions on Film Composition and Luminescence Properties. Chem Mater 12: 1305-1313.

44. Wahjudi PN, Oh JH, Salman SO, Seabold JA, Rodger DC, et al. (2009) Surface Engineering and Patterning Using Parylene for Biological Applications. Journal of Biomedical Materials Research Part A 89A: 206-214.

45. Eyvazov AB, Inoue IH, Stoliar P, Rozenberg MJ, Panagopoulos C (2013) Sci Rep p. 3.

46. Rui YF, Liu JQ, Yang B, Yang CS, Wei DX (2013) Electrodes for Nerve Recording and Stimulation. J Appl Electrochem 43: 301-308.

47. Marquez DT, Carrillo AI, Scaiano JC (2013) Visible and Near-Infrared Plasmon-Mediated Molecular Release from Cucurbit [6] uril Mesoporous Gated Systems. Langmuir 29: 10521-10528.

48. Ciriminna R, Fidalgo A, Pandarus V, Béland F, Ilharco LM et al. (2013) Towards waste free organic synthesis using nanostructured hybrid silicas. Chem Rev 113: 6592-6620.

49. Makarovsky I, Boguslavsky Y, Alesker M, Lellouche J, Banin E, et al. (2011) An Increased Efficiency of Triclosan Delivery by Novel Acrylate-Based Nanoparticles. Adv Funct Mater 21: 4295-4304.

50. Unger K, Rupprecht H, Valentin B, Kircher W (1983) The controlled release of tilmicosin from silica nanoparticles. Drug Dev Ind Pharm 9: 69-91.

51. Katsumoto Y, Komatsu H, Ohno K (2006) Building of Multifunctional and Hierarchical $HxMoO_3$/PNIPAM Hydrogel for High-efficiency Solar Vapor Generation. J Am Chem Soc 128: 9278-9279.

DOI: 10.32474/MAMS.2021.03.000173